β-1 Integrin-Mediated Adhesion May Be Initiated by Multiple Incomplete Bonds, Thus Accounting for the Functional Importance of Receptor Clustering

Joana Vitte, Anne-Marie Benoliel, Philippe Eymeric, Pierre Bongrand, and Anne Pierres
Laboratoire d'Immunologie, Institut National de la Sante et de la Recherche Medicale U600, Centre National de la Recherche Scientifique FRE2059, Hôpital de Ste-Marguerite, Marseille, France

ABSTRACT The regulation of cell integrin receptors involves modulation of membrane expression, shift between different affinity states, and topographical redistribution on the cell membrane. Here we attempted to assess quantitatively the functional importance of receptor clustering. We studied β-1 integrin-mediated attachment of THP-1 cells to fibronectin-coated surfaces under low shear flow. Cells displayed multiple binding events with a half-life of the order of 1 s. The duration of binding events after the first second after arrest was quantitatively accounted for by a model assuming the existence of a short-time intermediate binding state with 3.6 s^{-1} dissociation rate and 1.3 s^{-1} transition frequency toward a more stable state. Cell binding to surfaces coated with lower fibronectin densities was concluded to be mediated by single molecular interactions, whereas multiple bonds were formed <1 s after contact with higher fibronectin surface densities. Cell treatment with microfilament inhibitors or a neutral antiintegrin antibody decreased bond number without changing aforementioned kinetic parameters whereas a function enhancing antibody increased the rate of bond formation and/or the lifetime of intermediate state. Receptor aggregation was induced by treating cells with neutral antiintegrin antibody and antiimmunoglobulin antibodies. A semiquantitative confocal microscopy study suggested that this treatment increased between 40% and 100% the average number of integrin receptors located in a volume of $\sim$0.045 μm^3 surrounding each integrin. This aggregation induced up to 2.7-fold increase of the average number of bonds. Flow cytometric analysis of fluorescent ligand binding showed that THP-1 cells displayed low-affinity β-1 integrins with a dissociation constant in the micromolar range. It is concluded that the initial step of cell adhesion was mediated by multiple incomplete bonds rather than a single equilibrium-state ligand receptor association. This interpretation accounts for the functional importance of integrin clustering.

INTRODUCTION

Many cell functions are dependent on their capacity to control adhesive interactions. A prominent example is provided by the immune system and the complex migratory patterns displayed by lymphoid and myeloid cells after an antigenic challenge.

Many strategies are currently used to control cell adhesion. These include: i), adaptation of the repertoire of adhesive receptors through membrane translocation of stored molecules (Jagels et al., 1995), de novo biosynthesis (Gailit et al., 1996), or alteration of the rate of receptor removal (Condic and Letourneau, 1997); ii), modulation of the intrinsic affinity of membrane receptors through conformational changes (Ma et al., 2002), proteolytic events (Van de Winkel et al., 1989), or variation of glycosylation patterns (Skelton et al., 1998); and iii), alterations of the cell receptor relationship with the membrane environment. The latter processes that may be denominated as postreceptor (Danilov and Juliano, 1989) or perireceptor events may involve an increase of receptor accessibility through concentration into convex parts of the cell surface such as the tip of microvilli (Erlandsen et al., 1993), partial degradation of repulsive molecular structures composing the glycocalyx (Sabri et al., 2000), release of cytoskeletal constraints resulting in increased capacity to diffuse toward ligands on interacting surfaces (Kucik et al., 1996), or on the contrary increased strength of connection with surrounding membranes resulting in higher capacity to maintain adhesion in the presence of disrupting forces (Dwir et al., 2001; Leid et al., 2001).

Much recent evidence supported the view that receptor clustering is frequently involved in the regulation of adhesion. Whereas dimerization of selectins (Li et al., 1998), members of the immunoglobulin superfamily such as ICAM-1 (Miller et al., 1995), or mucin-like selectin ligands such as PSGL-1 (Sako et al., 1993) may be important to ensure the functional efficiency of these adhesion receptors, clustering seems a dynamic way of regulating adhesive interactions mediated by cadherins (Lino et al., 2001) and most importantly integrin receptors (van Kooyk and Figdor, 2000); thus, although it has long been known that integrin complement receptor CD11bCD18 was inactive on resting phagocytes, neutrophil exposure to suitable stimuli such as phorbol ester resulted in concomitant increase of cell capacity to bind complement-coated particles and clustering of receptors into small aggregates of 2–6 molecules (Detmers et al., 1987). Much evidence was also reported on the correlation between functional activation and membrane

Submitted December 17, 2003, and accepted for publication February 26, 2004.

Address reprint requests to Professor Pierre Bongrand, Tel.: +33-491-26-03-31; Fax: +33-491-75-73-28; E-mail: bongrand@marseille.inserm.fr.

0006-3495/04/06/4059/16 $2.00

doi: 10.1529/biophysj.103.038778

clustering of CD11aCD18/LFA-1, another β-2 integrin (van Kooyk et al., 1994; Stewart et al., 1998). Other reports support the hypothesis that β-1- (Grabovsky et al., 2000; Maheshwari et al., 2000) and β-3- (Kasirer-Friede et al., 2002) integrin clustering also influences functional capacity.

Although there is ample evidence that receptor clustering per se can enhance adhesion (Hermanowski-Vosatka et al., 1988; Yap et al., 1997; Hato et al., 1998), the molecular mechanisms responsible for this enhancement remain to be determined. At least three different mechanisms may be considered: first, binding site formation might require receptor multimerization, as was hypothesized for cadherins (Shapiro et al., 1995). Second, receptor clustering might trigger intracellular signaling events, such as tyrosine phosphorylation (Hato et al., 1998; Stripack et al., 1999). Third, clustered receptors might form multivalent bonds with surfaces bearing a sufficient density of ligand molecules, and multivalency would be required to achieve significant attachment that might be conducive to subsequent strengthening.

Although there is little doubt that the association of multiple weak bonds is a common way of achieving significant molecular interactions (Takaki et al., 2002), there remains to assess the quantitative consequence of multivalent association on the lifetime and mechanical strength of attachment. This is by no means a trivial question, as demonstrated in a recent theoretical study (Seifert, 2000); indeed, in absence of force, the lifetime of an attachment mediated by multiple parallel molecular bonds may be comparable to the lifetime of a single bond or much higher depending on the possibility of rebinding during the detachment process. Also, if a disruptive force is applied, the lifetime of a multimolecular attachment will be strongly dependent on the sharing of this force between individual bonds. Further, direct experimental determination of the effect of receptor clustering on adhesive efficiency may yield fairly inconclusive data. Thus, Chen and Moy (2000) used atomic force microscopy to determine the force required to break attachment between concanavalin-A-coated surfaces and control cells or cells expressing concanavalin-A ligand cross-linked with glutaraldehyde. Although cross-linking resulted in significant increase of the unbinding force (from 82 to 125 pN), it is difficult to determine whether this increase was a direct consequence of multivalent binding rather than increased cell rigidity or strengthening of the anchoring of cell surface molecules.

In this article, we describe a quantitative study of the effect of receptor clustering on the initial step of adhesion. We chose as a model the interaction of human monocytic THP-1 cells with fibronectin-coated surfaces; binding is mediated by low-affinity interactions involving $\alpha 4\beta 1$ and $\alpha 5\beta 1$ integrins (Faull et al., 1993). Three sets of measurements were performed. First, the surface topography of cell surface integrins was manipulated by cross-linking with a monoclonal antibody that did not alter integrin affinity state, and receptor clustering was studied quantitatively by combining immunofluorescence, confocal microscopy, and image analysis. Second, receptor binding affinity was controlled with a modification of standard Scatchard analysis. Third, the effect of receptor clustering on adhesive efficiency was assessed by monitoring transient attachment events displayed by cells driven along fibronectin-coated surfaces in a laminar flow chamber. This chamber was operated under very low shear stress so that a single molecular bond might provoke a detectable arrest. This procedure was previously demonstrated to allow quantitative analysis of initial binding events, independently of postreceptor phenomena (Pierres et al., 1994) and it yielded a quantitative estimate of the lifetime of bonds formed by selectins (Kaplanski et al., 1993) or integrins (Masson-Gadais et al., 1999) borne by living cells. Here we found that fairly extensive receptor clustering resulted in significant change of the lifetime of initial cell-surface binding events. Detailed analysis of the duration of these binding events under diverse experimental conditions strongly supported the hypothesis that initial cell arrests were mediated by short-lived transient molecular interactions. This might explain the need for simultaneous formation of multiple ligand-receptor interactions to achieve sufficient avidity.

MATERIALS AND METHODS

Cells and surfaces

We used the human monocytic THP-1 line (Tsuchiya et al., 1980). Cells were maintained as previously described (Sabri et al., 2000) in RPMI-1640 medium (Invitrogen, Cergy Pontoise, France) supplemented with 10% fetal calf serum (Invitrogen), 2 mM L-glutamine, 50 U/ml penicillin, and 50 μg/ml streptomycin. As checked with flow cytometry (not shown), these cells express CD49dCD29 (VLA-4) and CD49eCD29 (VLA-5) β-1 integrins.

Sterile plastic coverslips (10.5 $\times$ 22 mm^2, Thermanox Ref 179434, Nalge Nunc International, Rochester, NY) were incubated for 2 h in pH 7.2 phosphate buffered saline buffer containing 10 μg/ml, 1 μg/ml, or 0.1 μg/ml human fibronectin (ref F6277; Sigma Aldrich France, St. Quentin Fallavier, France). They were washed extensively before use.

In some experiments, microfilaments were altered by treating cells for 15 min before adhesion tests with 10 μg/ml cytochalasin D (Sigma Aldrich) or 0.3 μM latrunculin A (Calbiochem, Merck Eurolab, Darmstadt, Germany)

Receptor aggregation and labeling

In some experiments, cells were treated with monoclonal antibodies specific for integrin β-1 chain: 12G10 (a mouse IgG1 supplied by Serotec, Cergy Saint-Christophe, France) is known as a function-enhancing antibody whereas K20 is a neutral mouse IgG2a supplied by Beckman-Coulter-Immunotech (Marseille, France). Cell pellets were incubated in 25 μl of antibody solution for 30 min in RPMI supplemented with 1 g/l bovine albumin in ice bath. Integrin aggregation was induced by adding 25 μl of goat anti-mouse immunoglobulin (Immunotech, Marseille, France).

Deaggregated fluorescent antibodies were obtained by 45-min centrifugation (80,000 g) in a L7 Beckmann ultracentrifuge. Pellets were discarded and protein concentration was determined by measuring absorbance at 280 nm wavelength and using 1.46 as the optical density of 1 mg/ml immunoglobulin solutions (Mishell and Shiigi, 1980).

Adhesion under flow: data acquisition

Our procedure was previously described (Masson-Gadais et al., 1999). Briefly, fibronectin-coated coverslips were glued to the bottom of a plexiglass block bearing a rectangular cavity of 17 × 6 × 1 mm^3 forming the chamber. Cells were suspended (1 million per ml) in RPMI 1640 medium supplemented with 10% fetal calf serum. They were then driven into the chamber with a 2-ml syringe mounted on an electric syringe holder (Razel Scientific Instruments, supplied by Bioblock, Illkirch, France). The wall shear rate G was calculated according to the standard formula: $G = 6\,Q/h^2w$, where Q is the flow rate (in mm^3/s), whereas h and w are the chamber height (1 mm) and width (6 mm), respectively. A standard value of $G = 4\ s^{-1}$ was used throughout all experiments. The advantage of using such a low flow rate is that the hydrodynamic drag exerted on a cell bound to the surface is ~5 pN, as obtained by modeling the cell as a sphere of 6-μm radius and using standard results from fluid mechanics (Pierres et al., 1996). Therefore, a single ligand-receptor bond should be able to maintain a cell at rest during a detectable amount of time, thus allowing direct visualization of individual molecular interactions (Pierres et al., 2001).

The chamber was set on the stage of an inverted microscope (Olympus IX, Olympus, Melville, NY) equipped with a charge-coupled-device video camera (Model SPT M208CE, Sony, Clichy, France). Observation was performed with a 10× objective and 1.5× additional magnification. In a typical experiment, the flow was recorded for 10 min in a selected microscope field with a VHS tape recorder for delayed analysis. The recorder output was connected to a PCVision+ digitizer (Imaging Technology, Bedford, MA) mounted on an IBM-compatible desk computer. This allowed real-time digitization yielding 512 × 512 pixel images with 256 gray levels. A custom-made software allowed tracking of the front edge of moving cells with a sampling frequency of ~20/s (Kaplanski et al., 1993; Masson-Gadais et al., 1999). Pixel size was 0.6 μm along the trajectory axis. A typical trajectory is displayed on Fig. 1. Each videotape was replayed a sufficient number of times to monitor the motion of every cell passing through the microscope field during the recording period of time.

Adhesion under flow: data analysis and statistical treatment

Under each tested experimental condition, a typical number of 300–500 individual cell trajectories were monitored for determination of: i), sum L of the lengths of individual trajectories; ii), total number N of arrests; and iii), duration of each individual arrest.

Binding frequency

The binding frequency P was calculated as the ratio between the number N of (transient or durable) arrests and total displacement L ($P = N/L$). The accuracy of determination of this parameter was quantified by using $N^{1/2}/L$ as an estimate of the standard deviation σ_P, based on Poisson law (Masson-Gadais et al., 1999).

Dissociation rate

The durations of individual arrests detected in a given set of experiments were ordered, yielding a sequence such as:

$$t_1 < t_2 < \ldots < t_i < \ldots < t_N \quad (1)$$

where t_i is the duration of the ith arrest out of a total of N. The fraction $F(t)$ of cells remaining bound at time t_i after arrest is thus simply $(N - i)/N$. If all arrests were mediated by single bonds with first-order dissociation kinetics and dissociation rate k_{off}, $\ln(F(t))$ would be linearly dependent on time according to the simple equation:

$$\ln(F(t)) = -k_{off}t. \quad (2)$$

However, as exemplified on Fig. 2, experimental dissociation plots of $\ln(F(t))$ versus time were not straight lines. These plots were found to be adequately described with two parameters:

1. The initial dissociation rate d was calculated as the average slope within the time interval [0.15 s, 0.45 s] (see Results section for the explanation of this choice):

$$d = [\ln(F(0.15)) - \ln(F(0.45))]/[0.45 - 0.15]. \quad (3)$$

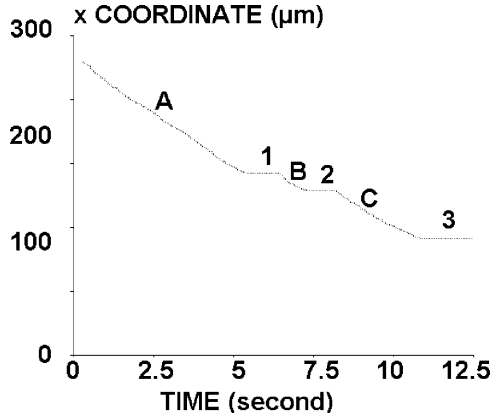

FIGURE 1 Motion of THP-1 cells along fibronectin-coated surfaces under flow. Monocytic THP-1 cells were driven along fibronectin-coated surfaces with a low wall shear rate of ~4 s^{-1}. A typical trajectory is shown: periods of fairly uniform motion (*A*, *B*, and *C*, with average velocities of 20.4 μm/s, 18.6 μm/s, and 16.8 μm/s, respectively) are separated by arrests of varying duration (*1* and *2* are transient arrests lasting 1.03 s and 0.95 s, respectively, *3* is a durable arrest (only partially shown in the figure)).

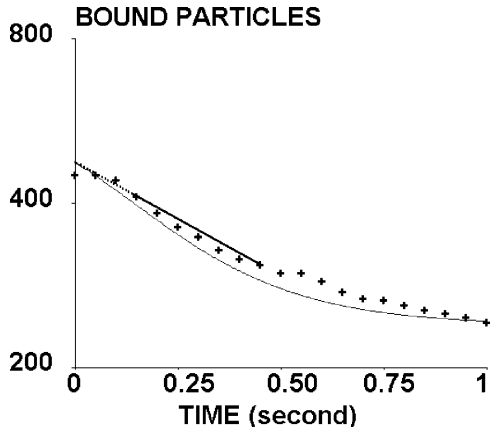

FIGURE 2 Duration of cell-fibronectin association. Monocytic THP-1 cells moving along fibronectin-coated surfaces displayed binding events with a wide range of durations. This figure shows a typical detachment curve obtained after recording 448 arrests on 1226 control cells interacting with surfaces coated with 10 μg/ml fibronectin. Experimental values are shown as crosses. Three domains could be defined: i), initial horizontal part that usually displayed downward concavity; ii), linear region where a corrected number of arrests could be obtained by extrapolation of the linear regression line (*thick line*); and iii), curved region revealing delayed bond stabilization (between 0.45 and 1 s after arrest).

To quantify the uncertainty of dissociation rate determination, the standard deviation σ_d was estimated as previously described by assuming Poisson distribution for the numbers A and B of arrests with duration within time intervals [0.15 s, 0.45 s] and [0.45 s, ∞], respectively (Pierres et al., 2002), yielding the formula:

$$\sigma_d = [A/B(A+B)]^{1/2}/(0.45-0.15). \quad (4)$$

2. The fraction of particles remaining bound at time one second r, was obtained by dividing the number of arrests lasting 1 s or more (C) by the estimated number of arrests N obtained by extrapolation to time zero of the dissociation plot (see Results section). The standard deviation for parameter $r = C/N$ was calculated as prescribed by Snedecor and Cochran (1980):

$$\sigma_r = (C \times (N-C)/N^3)^{1/2}. \quad (5)$$

The aforementioned formulae were used to assess the significance of differences between two experimental dissociation plots obtained under different experimental conditions by applying a standard chi-square test (with two degrees of freedom) to the following sum of squares:

$$\chi^2 = (d-d')^2/(\sigma_d^2+\sigma_{d'}^2) + (r-r')^2/(\sigma_r^2+\sigma_{r'}^2). \quad (6)$$

Note that the limiting values of χ^2 with one and two degrees of freedom are, respectively, 3.84 and 5.99 for a confidence level of 0.05.

Comparison of experimental dissociation plots with theoretical models

As previously reported (Kaplanski et al., 1993; Pierres et al., 1995; Zhu et al., 2002), the interpretation of dissociation plots is not straightforward due to the possible occurrence of two main phenomena.

First, when a first bond triggered a cell arrest, sequential bond formation and dissociation events may occur. The simplest model allowing one to account for this possibility consists of defining the rates of bond formation (k_{on}) and dissociation (k_{off}) and writing the following set of equations (Cozens-Roberts et al., 1990; Kaplanski et al., 1993):

$$dP_i(t)/dt = k_{on}[P_{i-1}(t) - P_i(t)] + k_{off}[(i+1)P_{i+1}(t) - iP_i(t)], \quad (7)$$

where $P_i(t)$ is the probability that the cell be bound by i bonds at time t. This set of master equations was solved numerically by proper truncation assuming that the total bond number remained lower than or equal to 10 during the first second after arrest. This model will be designated as the multiple-bond model with continuous bond formation, during the remaining part of this article. A natural assumption is that $P_i(0) = \delta_{1i}$, where δ is Kronecker's symbol.

It was recently found (Pierres et al., 2002) that better fit between experimental and calculated plots might be obtained with the so-called multiple-bond model with instantaneous bond formation: following this model, k_{on} is set equal to zero. Further, according to Poisson law:

$$P_i(0) \text{ is } \lambda^i \exp(-\lambda)/[1-\exp(-\lambda)]/i!, \quad (8)$$

where λ represents an average bond number that will be referred to as Poisson parameter. The underlying assumption is that several bonds may be formed within less than a fraction of a second if several ligand-receptor couples are at binding distance when cell-surface contact occurs.

Second, it is now well documented that a single ligand-receptor complex may undergo different states with different lifetimes (Pierres et al., 1995, 2002; Merkel et al., 1999). The simplest way of accounting for this possibility consisted of assuming that each cell arrest resulted from the formation of a transient complex with dissociation rate k_{off} and rate of transition k_t toward a stable state (i.e., a binding state with a lifetime much higher than 1 s). The basic equations can be solved analytically when there is a single bond (Pierres et al., 1995). A set of master equations resembling Eq. 9 can be obtained by defining as $P_{i,j}(t)$ the probability that a cell be bound by i transient-state interactions and j stabilized interactions at time t. The standard equation is:

$$dP_{i,j}(t)/dt = k_t[(i+1)P_{i+1,j-1}(t) - iP_{i,j}(t)] + k_{off}[(i+1)P_{i+1,j}(t) - iP_{i,j}(t)] + k_{2m}[(j+1)P_{i-1,j+1}(t) - jP_{i,j}(t)]. \quad (9)$$

The simplest two-parameter model was obtained by considering only the off rate of the transient state (k_{off}) and the transition rate k_t from intermediate to stabilized state. In some cases, it was found necessary to account for the reversion rate k_{2m}, i.e., the rate of passage from stabilized to transient interaction.

Numerical solution of this set of equations was straightforward, with proper truncation by limiting at 10 the maximum number of cell-substrate bonds during the first second after arrest.

A third model was based on the hypothesis that cell attachment might be mediated by two different kinds of complexes with dissociation rates $k_{off,A}$ and $k_{off,B}$, respectively. After straightforward calculations, the binding probability at time t is:

$$P(t) = r\exp(-k_{off,A}t) + (1-r)\exp(-k_{off,B}t), \quad (10)$$

where r is the proportion of type-A complexes, which should range between 0 and 1. Note that this minimal model uses three fitted parameters.

Assessment of receptor aggregation with confocal microscopy

Data acquisition

Receptor aggregation was assessed semiquantitatively by taking advantage of the exquisite sensitivity of confocal microscopy. Indeed, this device was found to detect a few or even single fluorescent molecules (Nie et al., 1994). Under standard conditions, cells were labeled in the cold with fluorescein-conjugated anti-CD29 mouse monoclonal antibodies as previously described, with or without a second layer of unlabeled polyclonal goat anti-mouse immunoglobulin. They were then fixed with 1% paraformaldehyde and examined rapidly with a confocal laser fluorescence microscopy (Leica CLSM, Leica Microsystems, Heidelberg, Germany), using an Argon/Krypton laser (Omnichrome, Leica) and a 40× dry objective. Pixel size was thus 245 × 245 nm^2 with a vertical resolution of order of 700 nm. Typically, a given cell was represented as a series of about six 512 × 512 pixel images (8-bit depth) with 2-μm separation between sequential section planes. It was found convenient to set detection photomultiplier at a moderate value of ~600 volts so that the background level is sufficiently low to avoid any confusion between random noise and fluorescence of volume elements containing a few labeled molecules.

To relate the fluorescence intensities of individual pixels to local density of fluorescent molecules (Pierres et al., 1994), 10 μl aliquots of sequential dilutions of fluorescent antibodies were deposited on glass slides and covered with 22 × 22 mm^2 coverslips, thus forming a liquid layer of ~20-μm thickness that was examined with the same microscope settings as cell samples.

Data processing

Images were transferred to desktop computers with a local network and processed with a custom-made image analysis software (André et al., 1990). Conventional observation of cell images would convey a misleading grasp of molecule aggregation because visible bright points represented large molecular aggregates representing only a small fraction of the total amount of receptors. Small cluster aggregation was assessed by calculating a median fluorescence aggregation index defined as the fluorescence intensity f such that 50% of fluorescent molecules are located in pixels with a brightness lower than f. This may be viewed as a weighted median fluorescence because the following equation holds:

$$\sum_{i=b}^{f} i \times n(i) = \sum_{i=f+1}^{255} i \times n(i), \tag{11}$$

where b is the background fluorescence intensity, as measured on a buffer solution, and $n(i)$ is the number of image elements with fluorescence brightness i. Thus, this index should yield a semiquantitative estimate of the median number of fluorescent molecules located in a volume element surrounding a given molecule. As shown in the results section, this index may be strongly affected by spontaneous aggregation of fluorescent antibodies.

Study of receptor affinity with soluble ligand molecules

To achieve correct interpretation of experimental data, it was important to check the effect of receptor aggregation treatment on their affinity. Thus, we studied the binding of two custom-made fluorescent integrin ligands by THP-1 cells: fluorescein-AEILDVPST contains the LDVPS sequence recognized by VLA-4 in the CS-1 domain of fibronectin (Mould and Humphries, 1991). Fluorescein-AGRGDSPK contains the RGD sequence found in the fibronectin region recognized by VLA-5 (Wayner et al., 1989). These molecules were supplied by Neosystem (Strasbourg, France).

Experiments were conducted by incubating cell pellets in 50 μl of sequential twofold dilutions of peptide ligand with concentration ranging between 0.38 μg/ml and 200 μg/ml. They were then examined with a Coulter EPICS/XL flow cytometer (Beckmann-Coulter France, Villepinte) for determination of relative median fluorescence.

Data analysis was performed with a modification of Scatchard procedure (Scatchard, 1949): the basic assumption is that the mean fluorescence F of a cell incubated in a solution of fluorescent ligand of concentration $[L]$ is:

$$F = F^\circ + \alpha[L] + Tf \times \{K_a[L]/(1 + K_a[L])\}. \tag{12}$$

The first term on the right-hand side of Eq. 12 is cell autofluorescence, the second term represents nonspecific binding that is assumed to be linearly dependent on ligand concentration, and the third term represents specific binding, defining T as the total number of binding sites on the cell, f as the intrinsic fluorescence of a ligand molecule, and K_a the affinity constant of ligand receptors. Equation 12 may be written:

$$1/\{(F - F^\circ)/[L] - \alpha\} = [L]/Tf + 1/K_aTf. \tag{13}$$

Because the receptor affinity was low enough to make the amount of bound ligand negligible with respect to the total amount of fluorescent ligand, $[L]$ was readily derived from the known concentration of fluorescent ligand solution. Further, $F - F^\circ$ was calculated by mere subtraction of the fluorescence of unlabeled cells samples. Finally, constant α was approximated as the limit of $(F - F^\circ)/[L]$ for high-ligand concentration: this limit was determined by calculating the average value of $(F - F^\circ)/[L]$ corresponding to three to four values of $[L]$ ranging between 50 μg/ml and 300 μg/ml (i.e., $\sim 5\ 10^{-5}$ and $3\ 10^{-4}$ M), which was much higher than the dissociation constant $1/K_a$. Parameters K_a and Tf were then determined with the Scatchard procedure by plotting $1/\{(F - F^\circ)/[L] - \alpha\}$ versus $[L]$ and determining the equations of the regression line in the ligand concentration range $[0, 10\,\mu\text{g/ml}]$.

Determination of fibronectin surface density

Mouse anti-human fibronectin monoclonal antibody HFN 7.1 was purified from hybridoma culture supernatants (American Type Culture Collection CRL-1606) and labeled with the Alexa Fluor protein labeling kit provided by Molecular Probes (Eugene, OR) as indicated by the supplier. Fibronectin-coated surfaces were treated with Alexa-Fluor 488-conjugated antibodies and fluorescence surface density was determined with confocal microscopy. Calibration was achieved by measuring the fluorescence of 5-μl samples of serial dilutions of labeled antibody deposited on a glass slide and covered with 10.2×22 mm^2 coverslips.

RESULTS

THP-1 cells moving along fibronectin-coated surfaces display numerous arrests that are essentially mediated by CD49eCD29 integrin receptors

In a preliminary set of experiments, control or antibody-treated THP-1 cells were driven along fibronectin surfaces under microscopical observation; numerous binding events were observed and arrest frequencies are shown on Table 1. Binding frequency was comparable in controls and cells that had been preincubated with IgG1 immunoglobulins, or anti-CD32 antibodies, however, antibodies known to block β-1 integrin receptors decreased binding frequency by 86% (antibody Lia 1/2) and 57% (3S3).

Because THP-1 cells were found to express two fibronectin receptors (i.e., CD49dCD29 and CD49eCD29, not shown) adhesion specificity was further studied with anti-CD49d and anti-CD49e antibodies; as shown in Table 1, binding frequency exhibited 19%, 76%, and 81% inhibition when cells were respectively treated with anti-CD49d, anti-CD49e, and a mixture of anti-CD49d and anti-CD49e.

TABLE 1 Specificity of THP-1/fibronectin interaction under flow

Antibody used	Number of cells	Binding frequency (mm^{-1})
None (control)	280	2.1 ± 0.14 (SE)
Control IgG1	50	2.3 ± 0.37 (SE)
Anti-CD32	242	2.0 ± 0.16 (SE)
Anti-CD29 (Lia 1/2)	156	0.3 ± 0.06 (SE)
Anti-CD29 (3S3)	101	0.9 ± 0.14 (SE)
Anti-CD49d (HP2/1)	154	1.7 ± 0.17 (SE)
Anti-CD49e (SAM1)	165	0.5 ± 0.08 (SE)
Anti-CD49d +Anti-CD49e	109	0.4 ± 0.08 (SE)

Monocytic THP-1 cells were driven along plastic coverslips that had been pretreated with 10 μg/ml human fibronectin for determination of the binding frequency. Experiments were done with controls, cells pretreated with irrelevant antibodies, and adhesion blocking antibodies specific for integrin β-1 chain (CD29), α4 (CD49d), or α5 (CD49e). Binding frequencies are shown ± SE (calculated as explained in the Materials and Methods section) together with the number of monitored cells.

It is concluded that adhesion was essentially mediated by CD49eCD29 ($\alpha5\beta1$) integrin under our experimental conditions.

The duration of binding events display wide variations, ranging between a fraction of a second and more than several minutes

As exemplified in Fig. 1, monocytic THP-1 cells driven along fibronectin-coated surfaces with low hydrodynamic forces exhibited periods of motion with fairly uniform velocity interspersed with arrests of varying duration. The distribution of arrest durations was determined for several experimental conditions. The detachment plot obtained after recording 448 arrests on a series of 1226 control THP-1 cells moving along surfaces pretreated by 10 μg/ml fibronectin is shown on Fig. 2, revealing three sequential parts:

1. The initial part of the curve usually displayed downward concavity when time ranged between 0 and ~0.15 s. This was felt difficult to analyze because the reliability of experimental data was hampered by potential artifacts related to cell shape irregularities, as discussed below.
2. Detachment curves were usually fairly linear on a semi-logarithmic scale in the region between 0.15 s and ~0.45 s after arrest, corresponding to first-order detachment kinetics. Therefore, it seemed reasonable to estimate the actual number of binding events by extrapolation to time zero of the tangent to the detachment curve in the linear region (Fig. 2). The difference between the extrapolated and experimental number of arrests ranged between 13% and 40% following experimental conditions as described below.
3. When time was higher than 0. 45 s, detachment curves usually displayed upward concavity, indicating progressive reinforcement of the binding mechanism.

It is concluded that three quantitative parameters could be derived with sufficient robustness from experimental analysis of cell attachment and detachment: i), binding frequency, defined as the mean number of binding events per μm displacement, ii), initial detachment rate, defined as the slope of detachment curves in the time interval [0.15 s, 0.45 s], and iii), fraction of cells remaining bound 1 s after arrest. The experimental values of these parameters were determined under various conditions affecting surface ligand density or cell receptor and cytoskeleton status. Parameters obtained after monitoring 8582 individual trajectories are summarized in Table 2 and full detachment curves are displayed in Fig. 3. A total number of 2136 arrests were observed, and 52% of them were shorter than 1 s.

Interaction between THP-1 cells and surfaces treated with 1 μg/ml or 0.1 μg/ml fibronectin is likely to be initiated by single-bond events

Although the flow chamber methodology was previously demonstrated to be sensitive enough to detect single-bond events, it may be difficult to ensure that arrests observed in a given experimental situation are mediated by single bonds (Zhu et al., 2002). This question was addressed by modifying the surface density of fibronectin on coverslips. When the fibronectin concentration used to derivatize adhesive surfaces was decreased from 10 μg/ml to 1 μg/ml, the initial detachment rate displayed about twofold increase (Table 2). However, when fibronectin concentration was further decreased from 1 μg/ml to 0.1 μg/ml, binding frequency exhibited nearly fourfold decrease, whereas detachment curves were identical on a time period of 5 s (Fig. 3 *A*). Thus, arrests observed with the lower two fibronectin concentrations reflected minimal binding events, and they were assumed to represent single molecular bonds.

TABLE 2 Influence of antibodies and receptor aggregation on THP-1 cell adhesion to fibronectin under flow

Cell treatment	Fibronectin concentration	Number of cells	Number of arrests	Binding frequency (mm^{-1})	Initial detachment rate (s^{-1})	Fraction bound 1 s after arrest
None	10 μg/ml	1226	448	1.48 ± 0.07	0.96 ± 0.10	0.51 ± 0.023
K20	10 μg/ml	760	120	0.74 ± 0.07	1.64 ± 0.26	0.40 ± 0.043
K20+anti-mouse Ig	10 μg/ml	709	140	0.93 ± 0.08	1.18 ± 0.20	0.52 ± 0.042
12G10	10 μg/ml	390	97	1.21 ± 0.12	0.95 ± 0.21	0.57 ± 0.050
Cytochalasin D	10 μg/ml	624	100	0.79 ± 0.08	2.02 ± 0.32	0.28 ± 0.041
Latrunculin A	10 μg/ml	452	93	1.09 ± 0.11	2.23 ± 0.36	0.28 ± 0.042
None	1 μg/ml	607	87	0.75 ± 0.08	2.26 ± 0.40	0.27 ± 0.046
K20	1 μg/ml	941	115	0.45 ± 0.042	1.83 ± 0.29	0.36 ± 0.042
K20+anti-mouse Ig	1 μg/ml	707	205	1.19 ± 0.08	1.02 ± 0.14	0.55 ± 0.030
12G10	1 μg/ml	671	191	1.50 ± 0.11	0.81 ± 0.13	0.62 ± 0.034
None	0.1 μg/ml	1495	180	0.21 ± 0.02	1.94 ± 0.27	0.32 ± 0.037

Monocytic THP-1 cells were driven with low shear forces along surfaces pretreated with 10 μg/ml, 1 μg/ml, or 0.1 μg/ml fibronectin. Experiments were done with control cells, cells treated with neutral (K20) or function-activating (12G10) anti-β-1 chain, and cells treated with cytoskeleton-disrupting agents cytochalasin D and latrunculin A. Receptor aggregation was achieved by treating cells with K20, then anti-mouse $(Fab')_2$ antibodies. In each series of experiments, the binding frequency, initial detachment rate, and fraction of cells remaining bound 1 s after arrest were determined. Results are shown ± SE, which was calculated as explained. A total number of 8592 cells and 1776 arrests were recorded.

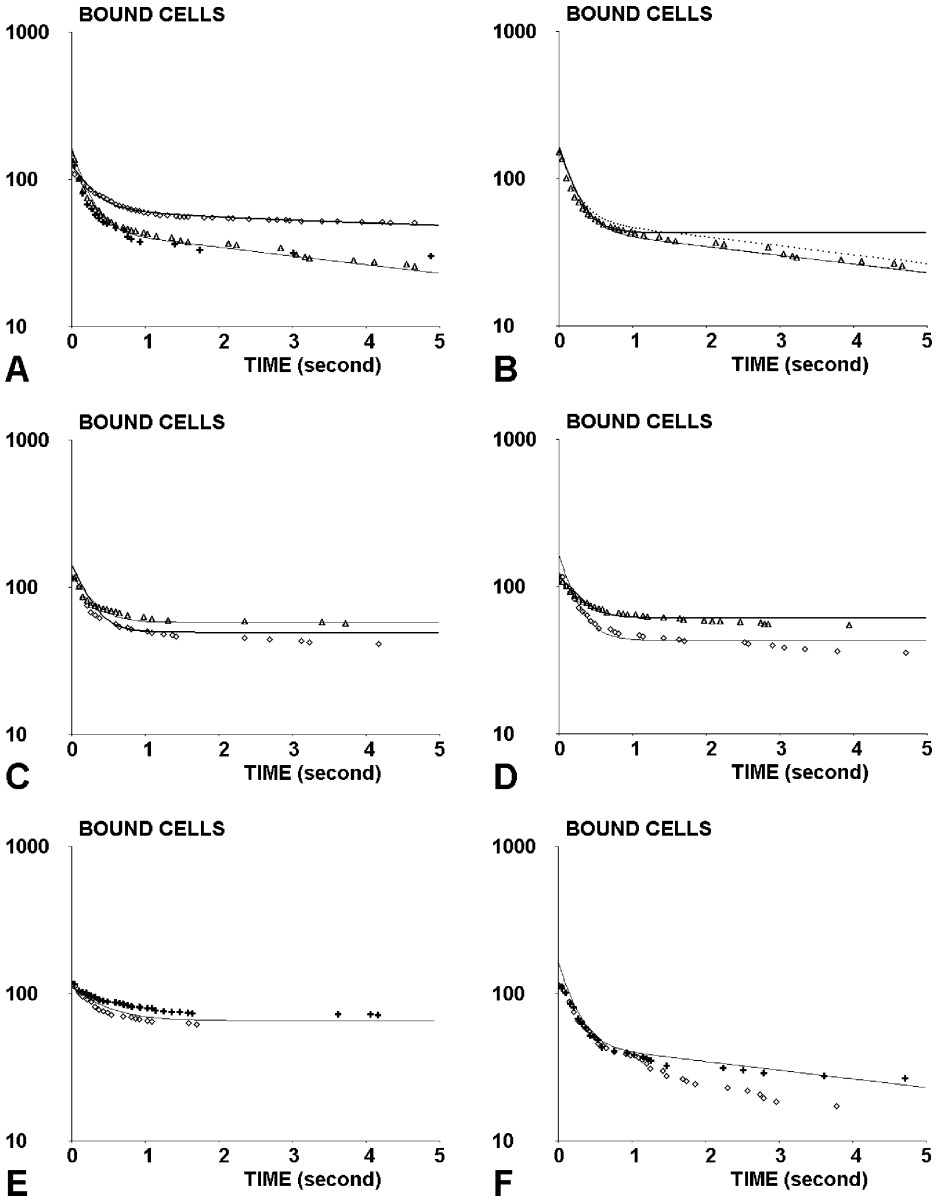

FIGURE 3 Summary of experimental data. A total number of 8582 cell trajectories were monitored and 1776 binding events were followed for at least 5 s each to determine their duration. Detachment curves obtained under various experimental conditions are shown together with a selection of theoretical curves. To allow optimal comparison, curves were normalized by setting at 100 the number of bound cells at time 0.15 s after arrest. (*A*) Control cells interacted with surfaces coated with 10 μg/ml (◇), 1 μg/ml (*crosses*), or 0.1 μg/ml (△) fibronectin. The thin line was obtained with a three-parameter model ($k_{off} = 3.6\ s^{-1}$, $k_t = 1.3\ s^{-1}$, $k_{2m} = 0.19\ s^{-1}$). The thick line was obtained with a five-parameter model derived from the previous one by allowing bond formation with kinetic rate $k_{on} = 1.44\ s^{-1}$ and average initial number of bonds 2.16. (*B*) Control cells interacting with surfaces coated with 0.1 μg/ml fibronectin. The thin line was obtained with the same three-parameter model as shown in *A*, the thick line was obtained with the simplest two-parameter model (single intermediate complex with off rate $k_{off} = 3.6\ s^{-1}$ and transition rate to more stable conformation $k_t = 1.3\ s^{-1}$). The dotted line was obtained with another three-parameter model, assuming that attachment might be mediated by two complexes with dissociation rates of $5.1\ s^{-1}$ (66%) or $0.137\ s^{-1}$ (34%). (*C*) Cells were treated with neutral K20 antibodies without (◇) or with (△) aggregation with anti-mouse immunoglobulins before studying interaction with surfaces coated with 10 μg/ml fibronectin. Theoretical curves were obtained with immediate bond-formation model, using previously determined parameters $k_{off} = 3.6\ s^{-1}$ and $k_t = 1.3\ s^{-1}$ with an average initial bond number of 1.52 (K20 only) or 2.47 (aggregated receptors). (*D*) Cells were treated with neutral K20 antibodies without (◇) or with (△) aggregation with anti-mouse immunoglobulins before studying interaction with surfaces coated with 1 μg/ml fibronectin. Theoretical curves were obtain with immediate bond-formation model, using previously determined parameters with an average initial bond number of 1 (K20 only) or 2.72 (aggregated receptors). (*E*) Cells were treated with 12G10 function-enhancing antibodies before studying interaction with surfaces coated with 10 μg/ml (◇) or 1 μg/ml (*crosses*) fibronectin. The theoretical curve was calculated assuming single bonds with two kinetic constants $k_{off} = 0.92\ s^{-1}$ and $k_t = 1.3\ s^{-1}$. (*F*) Cells were treated with cytochalasin D (◇) or latrunculin A (*crosses*) before interacting with surfaces coated with 10 μg/ml fibronectin . The theoretical curve was calculated with the same model as used in Fig. 3 *B* (single bond three-parameter model).

Detachment curves obtained with low-ligand density for time values lower than 1 s may be accounted for by assuming the existence of a transient ligand-receptor complex with a dissociation rate of 3.6 s^{-1} and a transition frequency of 1.30 s^{-1}

At least two nonexclusive mechanisms might account for the upward curvature of detachment curves (Fig. 3):

1. Additional bonds might occur after arrest. This situation may be modeled with a simple set of equations (see Eq. 7 in Materials and Methods) with two adjustable parameters, namely the association and dissociation rates, k_{on} and k_{off}. Parameter k_{on} is expected to decrease when the fibronectin surface density is decreased, whereas k_{off} should not be dependent on ligand density.
2. The initial molecular interaction might shift from a transient state to a stable one, thus allowing the introduction of two adjustable parameters, the dissociation rate of the intermediate state (k_{off}) and the transition frequency (k_t) defined as the frequency of shifting to a more stable state. Both parameters k_t and

k_{off} should be independent of fibronectin surface density.

Results displayed on Fig. 3 *A* suggest that no bond formation occurred after arrest at low-fibronectin density, because detachment curves found on surfaces treated with 1 μg/ml and 0.1 μg/ml fibronectin were identical. To check this hypothesis, we determined the numerical parameters yielding minimal value of the χ^2 difference (as calculated with Eq. 6) between theoretical curves and the detachment curve obtained with control cells interacting with surfaces coated with low (0.1 μg/ml) fibronectin concentration. The best fits obtained with both models are shown in Fig. 4. Clearly, a much better agreement was obtained with the bond-stabilization model ($\chi^2 = 0.003$) than with the multiple-bond model ($\chi^2 = 4.3$; $P < 0.05$). The fitted parameters were $k_{off} = 3.6\ s^{-1}$ and $k_t = 1.30\ s^{-1}$.

Detachment curves obtained with control cells and surfaces treated by 10 μg/ml fibronectin are accounted for by a multiple-bond model

The simplest way of interpreting the detachment curve obtained with THP1-cells interacting with surfaces treated with higher fibronectin concentrations was to allow multiple-bond formation and keep previously determined values of k_{off} and k_t. Two models might be considered: indeed, we could allow continuous bond formation after the formation of a first bond by introducing an association constant k_{on} (Eq. 7). This was called the continuous bond-formation model. Alternatively, assuming that multiple bonds could form immediately after contact (i.e., within <0.15 s), it was possible to make use of Eq. 7 with $k_{on} = 0$ and a probability distribution following Poisson law for the initial number of bonds (Pierres et al., 2002). This was called the immediate bond-formation model. As shown on Fig. 5, the immediate bond-formation model yielded slightly better χ^2 value (1.34; $P \approx 0.25$) than the continuous bond-formation model ($\chi^2 = 3.05$; $P < 0.10$). It may also be noticed that only the immediate bond-formation model yielded downward concavity of the initial part of detachment curves.

However, it must be emphasized that these models are nonexclusive, and excellent fit could be obtained by combining higher than one initial bond number and continuous bond formation.

Increasing complexity may be addressed by considering time values comprised between 0.15 and 5 s after initial arrest

As shown in Fig. 3 *B*, our two-parameter model ($k_{off} = 3.6\ s^{-1}$ and $k_t = 1.3\ s^{-1}$; *thick line*) did not satisfactorily account for single-bond rupture curves during the first 5 s after arrest. The most reasonable way of dealing with this discrepancy was to allow for the reversibility of bond strengthening by adding a transition frequency k_{2m} for the return from ''stable'' to transient state in single bonds. As shown in Fig. 3 *B*, excellent fit was obtained with $k_{2m} = 0.19\ s^{-1}$. Introducing this additional constant also allowed satisfactory account of detachment curves at high fibronectin surface density (Fig. 3 *A*). Interestingly, this change did not significantly affect the analyses performed on a narrower time interval of [0.15 s, 1 s]. However, because <10% of all arrests lasted between 1 and 5 s, k_{2m} could be estimated with only low accuracy. Thus, because we were essentially interested in the initial step of cell-surface interaction, it was found safer to restrict analyses to the shorter time interval

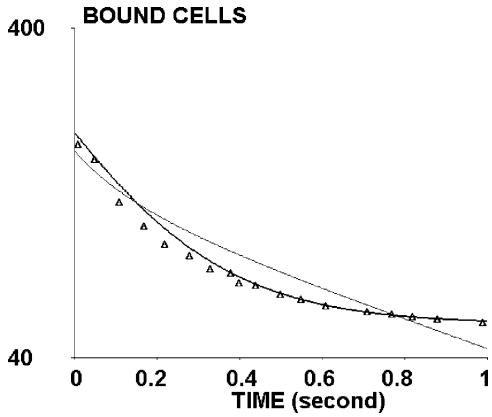

FIGURE 4 Interaction of control THP-1 cells with surfaces treated with lower fibronectin concentration. The interaction of control THP-1 cells with surfaces coated with 0.1 μg/ml fibronectin was studied. Triangles represent experimental values obtained after monitoring 1495 individual cells (180 arrests). The thick line was obtained with a single two-state bond model ($k_{off} = 3.6\ s^{-1}$ and $k_t = 1.3\ s^{-1}$). The thin line represents a theoretical curve obtained with multiple one-state bond model ($k_{off} = 3.18\ s^{-1}$, $k_{on} = 4.77\ s^{-1}$).

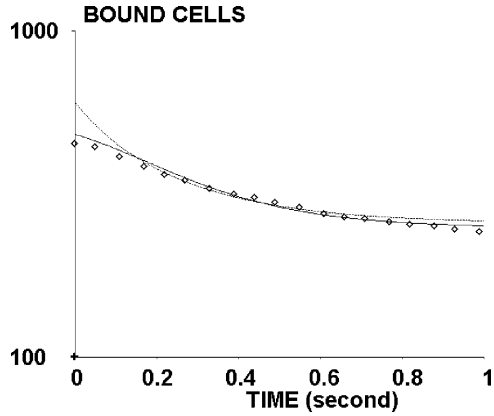

FIGURE 5 Interaction of control THP-1 cells with surfaces treated with higher fibronectin concentration. The interaction of control THP-1 cells with surfaces coated with 10 μg/ml fibronectin was studied. Diamonds represent experimental values obtained after monitoring 1226 individual cells (448 arrests). The thick line was obtained with the immediate bond-formation model average initial bond number: 2.64 ($k_{off} = 3.6\ s^{-1}$ and $k_t = 1.3\ s^{-1}$). The thin line represents a theoretical curve obtained with continuous bond-formation model ($k_{off} = 3.6\ s^{-1}$, $k_{-t} = 1.3\ s^{-1}$, $k_{on} = 3.96\ s^{-1}$).

[0.15 s, 1 s], to avoid interpretation problems due to the possibility of fitting curves with multiple combinations of parameters.

However, the above interpretation was not unique. Detachment curves could also be accounted for by a three-parameter model assuming that cell attachment might be mediated by two different complexes with dissociation rates $k_{off,A}$ and $k_{off,B}$ (Eq. 9). Taking for $k_{off,B}$ the average slope of the detachment curve (Fig. 3 *B*) on the time interval [1 s, 5 s], i.e., 1.37 s^{-1}, $k_{off,A}$, and the proportion r of type-A complex were fitted on time interval [0 s, 1 s] as described above. The dissociation rate $k_{off,A}$ was estimated at 5.1 s^{-1} and the proportion of arrests mediated by a type-A bond was 0.66, with a χ^2 parameter of 1.28, yielding a satisfactory agreement between experimental and theoretical values on the entire [0 s, 5 s] interval (Fig. 3 *B*, *dotted line*).

Clustering surface β-1 integrins on THP-1 cells with anti-mouse immunoglobulin increases binding frequency and duration of cell arrests on fibronectin-treated surfaces under flow

Integrin activity is difficult to study because it is known to be dependent on both molecular topography and conformation, and both parameters may be modulated by cell activation. We attempted to assess the specific consequences of topographical changes by selective manipulation of this parameter with neutral K20 antiintegrin antibody.

When K20-treated THP-1 cells were made to interact with surfaces coated with 1 μg/ml fibronectin (Fig. 3 *D*), experimental detachment curves were quite close to theoretical curves corresponding to the two-parameter model (k_{off} = 3.6 s^{-1}, k_t = 1.3 s^{-1}) because χ^2 was 0.93, and binding frequency displayed 40% decrease as compared to control cells (Table 2).

When K20-treated THP-1 cells interacted with surfaces coated with 10 μg/ml fibronectin, binding frequency was decreased by 50% as compared to controls, and the experimental detachment curve was slightly but significantly different from the aforementioned two-parameter single-bond model ($\chi^2 = 4.88$, as compared to $\chi^2 = 171$ for control THP-1 cells). The most straightforward interpretation of these experiments was that K20 antibody slightly decreased integrin accessibility under flow, but that it did not affect kinetic parameters, as expected.

In another set of experiments, THP-1 cells were first treated with K20 antibody, then exposed in the cold to polyclonal anti-mouse immunoglobulin to induce clustering of K20-treated integrins, and finally allowed to interact with fibronectin-coated surfaces. As shown in Table 2, this treatment resulted in both increase of binding frequency (2.6-fold; $P < 0.001$) and decrease of initial detachment rate (44%; $P < 0.05$) of THP-1 cells on surfaces treated with low fibronectin concentrations (1 μg/ml). When surfaces pretreated with higher fibronectin concentrations (10 μg/ml) were used, the same trend was observed, although neither binding frequency increase nor detachment rate decrease were significant.

Using the initial bond-formation model, the best fits between experimental and theoretical curves were obtained by assuming a mean initial bond number of 2.5 and 2.7 with aggregated integrins (on surfaces treated with 10 μg/ml and 1 μg/ml fibronectin, respectively), and 1.5 and 1 in the absence of integrin aggregation (on surfaces treated with 10 μg/ml and 1 μg/ml fibronectin, respectively).

Binding frequency and duration under flow are increased by function-enhancing 12G10 antibody

It was interesting to determine the influence on our experimental parameters of agents known to modify integrin conformation; as shown in Table 2, function-enhancing 12G10 antibody increased both binding frequency (twofold) and binding duration (2.8-fold) on surfaces coated with 1 μg/ml fibronectin, whereas no significant effect was found on surfaces coated with 10 μg/ml fibronectin.

As shown on Fig. 3 *E*, detachment curves determined on 12G10-treated cells were similar on surfaces coated with 10 μg/ml and 1 μg/ml fibronectin. Assuming that arrests were mediated by single bonds, optimal fit with theoretical curves was obtained with a k_{off} value of 0.915 s^{-1}, using unchanged $k_t = 1.3$ s^{-1} ($\chi^2 = 0.57$). Thus, the effect of 12G10 treatment might be accounted for by a nearly fourfold reduction of the dissociation rate of transient state. However, several different parameter combinations might yield similar results, and more studies would be required to determine the precise effect of 12G10 treatment on receptor-binding parameters.

The effect of microfilament inhibition may be accounted for by assuming decrease of receptor accessibility without any change of dissociation rate

Microfilament inhibitors have often been used to alter integrin function by modulating topographic distribution and mobility on the cell membrane. It was therefore interesting to quantitate the effect of such treatment on binding parameters measured under flow. As shown in Table 2, cytochalasin D and latrunculin A, respectively, decreased binding frequency by 47% and 26%. Both detachment curves matched our simple two-parameter single-bond model with χ^2 = 1.38 and 1.68, respectively, without any need for a change of parameters k_{on} and k_t (Fig. 3 *F*). The simplest interpretation of these results was that microfilament inhibition decreased receptor accessibility without any conformational change.

Receptor aggregation may be estimated with confocal microscopy

Experiments were performed to assess the capacity of confocal microscopy to monitor the aggregation of fluorescent

molecules. Serially diluted solutions of fluorescent anti-CD29 antibodies were examined with a confocal microscope as liquid sheets of ~20-μm thickness on a glass slide. As shown in Fig. 6, the average field brightness was linearly dependent on antibody concentration, and a 5-μg/ml concentration increase resulted in an increase of 1 unit on the 256 level intensity scale. Because the pixel size was 0.245 μm and vertical resolution was ~0.7 μm, the average number of molecules per pixel was ~0.8 for a 5-μg/ml solution. Thus, with our microscope settings, an intensity unit represented about one molecule of labeled immunoglobulin (i.e., two to three fluorescein groups) in a volume element (i.e., a voxel). Note that a 5-μg/ml fluorescent antibody solution appeared as completely dark on the microscope screen with standard color palette.

The image histogram could thus be used to monitor the size distribution of fluorescent molecules, as illustrated in a representative set of experiments shown in Fig. 7; when a control phosphate buffer solution was observed, nearly 95% of pixels had a brightness comprised between 2 and 3, corresponding to the background level, and 0.01% or less were brighter than 17. When a standard solution of fluorescent antibodies was studied, much wider brightness variations were observed, and the median fluorescence aggregation index (see Materials and Methods for definition) was 47. Finally, when aggregates were removed by ultracentrifugation, the median aggregation fluorescence index was 7, i.e., only 4–5 units above background level.

It was important to check that the spatial resolution of the confocal microscope was sufficient to prevent spreading of the fluorescence of individual aggregates into several neighboring pixels. As shown in Fig. 8, when the fluorescence intensities of individual pixels were read on the image of a nondeaggregated solution of fluorescent molecules,

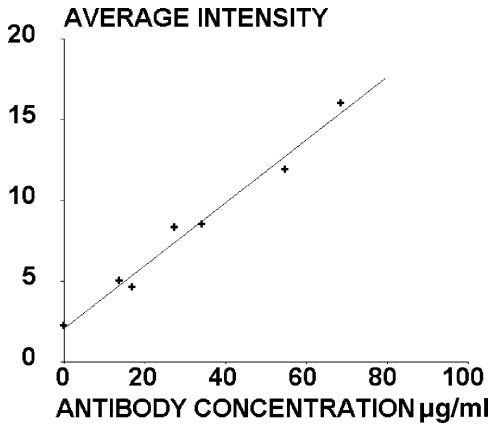

FIGURE 6 Absolute calibration of a confocal microscope. Serial dilutions of fluorescent antibodies were examined as parallelepipedic sheets, yielding fields of uniform brightness. The relationship between intensity and antibody concentration was fairly linear, as shown on a representative experiment. Correlation coefficient is 0.99; the regression line equation is: Intensity = 0.195 × concentration (μg/ml) + 2.06.

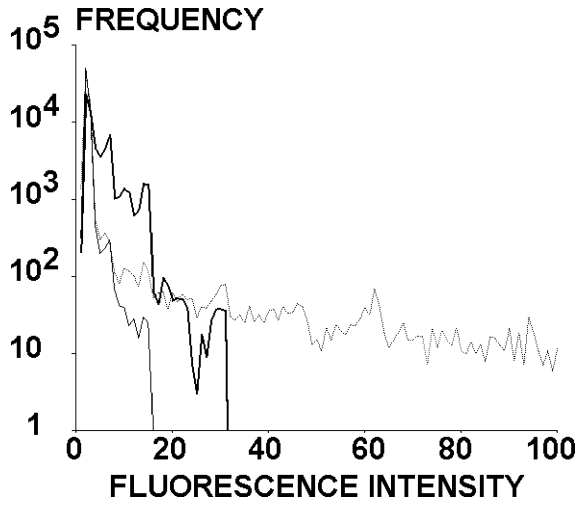

FIGURE 7 Spatial fluorescence distribution of fluorescent antibody solutions. Solutions of phosphate buffer (*thin line*), standard fluorescent antibodies (*dotted line*), or deaggregated fluorescent antibodies (*thick line*) were studied with confocal microscopy; the histogram of intensity distribution in a representative sample of 65,536 pixels is shown in each case.

which revealed a number of bright spots corresponding to molecular clusters, the brightest pixels remained surrounded by dark ones. Also, vertical resolution could be checked (not shown) by ensuring absence of correlation between the images of two parallel section planes of a cell.

Adding anti-immunoglobulin to cells treated with fluorescent CD29 monoclonal antibodies results in about twofold increase of median fluorescence index

Cells were treated with fluorescent anti-CD29 monoclonal antibodies, with or without additional exposure to anti-mouse immunoglobulin $(Fab')_2$ to relate measured kinetic binding parameters to fluorescence topography. Suspended cells were then fixed, and a series of confocal sections of labeled cells were examined quantitatively to gain some information on the membrane receptor organization at the onset of adhesive interactions such as were studied in the flow chamber: As shown on Fig. 9, measured fluorescent aggregation index was dependent on both the choice of the section plane and fluorescence distribution. When diametral section planes were selected, second antibody treatment resulted in a 1.5- to 2-fold increase of median fluorescence aggregation index, as summarized in Table 3.

Tested THP-1 cells express low-affinity fibronectin receptors

β-1 and β-2 integrins are known to display multiple affinity states depending on cell type and activation. It was thus

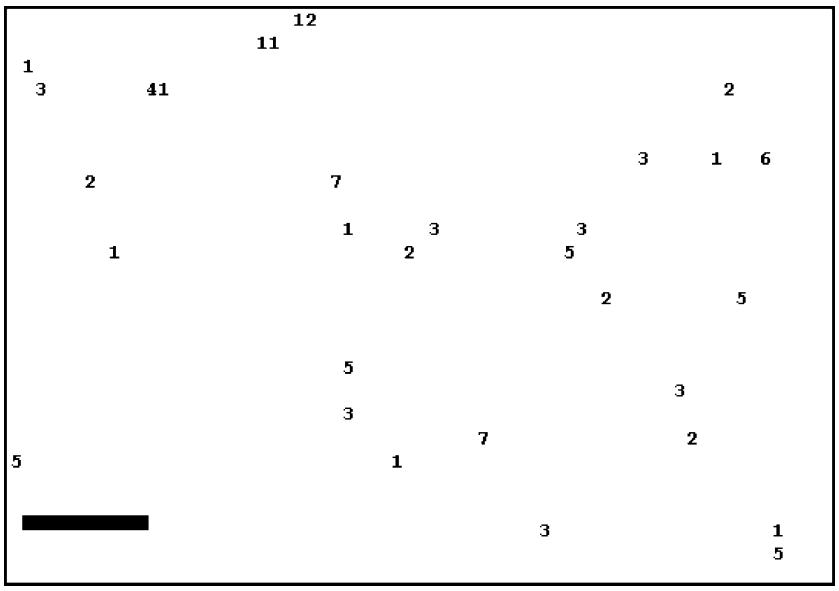

FIGURE 8 Spatial resolution of a confocal microscope. A nondeaggregated solution of fluorescent immunoglobulin molecules was observed with confocal microscopy, and the fluorescence of individual pixels is shown on a representative area. Values are expressed with a 16-level scale, and pixel with intensity <1 (i.e., <16 on a 256-level scale) are not shown for the sake of clarity. Obviously, there is no light spread around the brightest pixels. Bar is 2.5 μm.

important to obtain some information on the state of fibronectin receptors on THP-1 cells. This was performed with a modified Scatchard analysis, assuming linear dependency of nonspecific binding on free ligand concentration. As shown in Fig. 10, the validity of this assumption, as embodied by Eq. 11, was supported by experimental data. As summarized in Table 4, THP-1 cells bound both VLA-4 and VLA-5 ligands with low affinity, within the μM^{-1} range, and this was not substantially modified by neutral K20 antibody, as expected. It is thus concluded that THP-1 cells expressed low-affinity fibronectin receptors. However, the sensitivity of our technique was found insufficient to allow a safe comparison of the effect of different antibodies and treatments on receptor affinity and density.

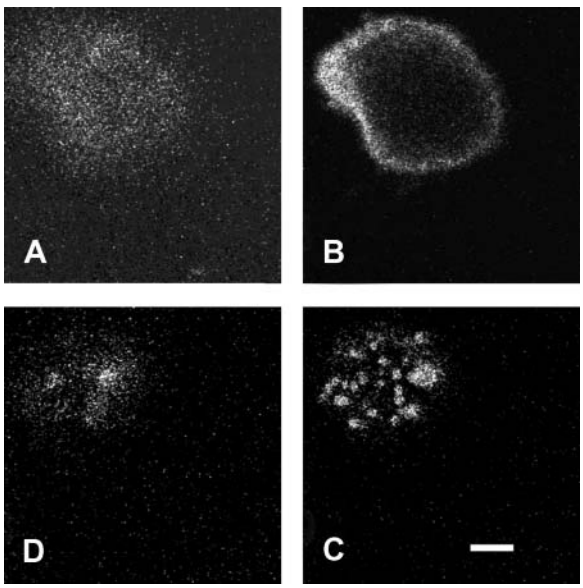

FIGURE 9 Influence of section plane and fluorescence distribution on the median fluorescence index. Monocytic THP-1 cells were labeled in suspension with fluorescent anti-CD29 monoclonal antibodies without (*A*, *B*) or with (*C*, *D*) additional anti-mouse immunoglobulin polyclonal $(Fab')_2$. They were then fixed and examined with confocal microscopy and representative sections corresponding to a diametral plane (*B*, *D*) or closer to the cell boundary (*A*, *C*) are shown. The mean fluorescence aggregation index was calculated as described to yield a semiquantitative estimate of receptor aggregation. Values obtained on these representative examples were respectively 6 (*A*), 16 (*B*), 12 (*C*), and 43 (*D*). Bar length is 5 μm.

Surface density of fibronectin on surfaces used to monitor adhesion

It was interesting to determine whether the binding behavior of fibronectin-coated surfaces was fully accounted for by the ligand surface density. Therefore, fluorescent anti-fibronectin antibodies were prepared and used to determine the surface density of fibronectin epitopes on different surfaces with confocal microscopy. The number of epitopes measured on surfaces coated with 10, 1, 0.1, and 0 μg/ml fibronectin were, respectively, 6500, 3850, 1436, and 0 (undetectable) sites/μm^2.

DISCUSSION

The essential purpose of this work was to present a microkinetic study of the interaction between fibronectin receptors and their ligand to assess the precise role of receptor clustering in functional regulation.

To clarify the significance of our findings, some methodological points deserve to be discussed. Although the use of flow chambers became more and more common in

TABLE 3 Effect of anti-mouse immunoglobulin on the fluorescence distribution of THP-1 cells labeled with fluorescent CD29 antibodies

	Median fluorescence aggregation index	
	F-anti-CD29	F-anti-CD29 + anti-mouse Ig
Experiment I	19.0 ± 1.84 ($n = 15$)	40.5 ± 7.2 ($n = 11$)
Experiment II	43.9 ± 4.1 ($n = 13$)	59.9 ± 3.7 ($n = 14$)

In two separate experiments, THP-1 cells were labeled with fluorescent monoclonal mouse anti-CD29 antibodies with or without unlabeled polyclonal anti-mouse $(Fab')_2$. The median fluorescence aggregation index was determined on diametral cell sections as explained in the Materials and Methods section. Mean values are shown ± SE of the mean (number of cells in brackets). The anti-mouse immunoglobulin significantly increased the mean fluorescence index ($P < 0.005$ in Experiment I and $P < 0.01$ in Experiment II) using *t*-test as described by Snedecor and Cochran (1980).

biological laboratories during the last 10 years, most authors used wall shear rates of the order of 100 s^{-1} or more (Lawrence and Springer, 1991) to mimic rheological conditions occurring in blood flow. In contrast, we operate the flow chamber at ~100-fold lower shear rates, leading to several interesting features.

1. The hydrodynamic force experienced by cells is of the order of a piconewton. This force is probably low enough to allow most ligand-receptor bonds to maintain flowing cells at rest for a detectable period of time. In contrast, probably only part of adhesion molecules such as selectins (Lawrence and Springer, 1991) or some integrins (Grabovsky et al., 2000) can withstand the higher forces usually exerted in flow chambers after an interaction shorter than a few milliseconds. Even in these cases there remains a possibility that reported first-order dissociation kinetics (Alon et al., 1995) be mediated by bond clusters rather than single bonds (Evans et al., 2001; Zhu et al., 2002). In any case, our conditions are certainly required to allow direct observation of the initial step of integrin-ligand interactions that would not be detected at higher shear rate (Lawrence and Springer, 1991).
2. In contrast with studies performed at high shear rate, freely flowing cells are very easy to monitor. Therefore, there is no difficulty in direct measurement of binding frequencies, i.e., the probability that a cell form a bond with the surface during a unit length displacement at binding distance.
3. However, using a low shear flow makes more difficult the detection of very transient arrests, particularly when adhesion studies are conducted with actual cells rather than spherical particles. Indeed, cell shape asymmetry may result in velocity fluctuations (Tissot et al., 1992) that may mimic adhesion-related arrests, and the cell boundary may not be determined with the same accuracy as the center of gravity of a sphere. Thus, it was deemed unwarranted to analyze the initial part ($t < 0.15$ s) of detachment curves.
4. In addition to its use as an analytical tool, the flow chamber operated at low shear rate may provide a suitable way of mimicking cell adhesion as occurs under many physiologically relevant situations. Indeed, cell membranes display continuous deformations corresponding to, e.g., lamellipodial extension and retraction. Using 20 nm as a reasonable receptor length, typical displacement rates of 1–10 μm/min would allow bond formation during contact periods of the order of 0.1–1 s. It is therefore useful to develop methods allowing experimental monitoring of cell attachment with 1-s resolution.

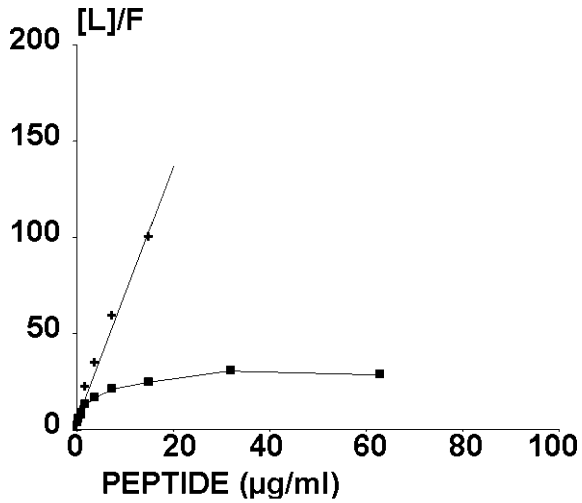

FIGURE 10 Validity of the linear approximation for nonspecific ligand binding. Monocytic THP-1 cells were incubated with an extensive concentration range of fluorescent peptide ligand specific for VLA-4 or VLA-5. Cell fluorescence F was determined with flow cytometry for each ligand concentration $[L]$. The dependence of $[L]/F$ on $[L]$ is shown after mere subtraction of cell autofluorescence (■) or subtraction of autofluorescence and nonspecific binding assumed to be linearly dependent on $[L]$ (*crosses*). The latter curve is linear, in accordance with Eq. 13.

Our analysis relies on the basic assumption that during the first second after arrest, binding events involving control cells interacting with lower ligand densities were mediated by single bonds. This assumption is supported by the following two arguments: i), it seems reasonable to assume that our methodology allowed single-bond detection; and ii), if more than one bond occurred during the first second after arrest, the average bond number would be significantly lower on surfaces coated with 0.1 μg/ml fibronectin than on surfaces coated with 1 μg/ml fibronectin, where binding frequency was nearly fourfold higher, and detachment kinetics should be different.

As shown in Fig. 3 *B*, at least two models might be considered to account for these results. First, fibronectin-integrin interaction might be initiated by the formation of a transient complex with a dissociation rate of 3.6 s^{-1} and 1.3 s^{-1} frequency of transition toward a more stable state with a lifetime much higher than 1 s. Alternatively, attach-

TABLE 4 Low-affinity state of fibronectin receptors expressed by THP-1 cells

Peptide ligand	Antibody added	Number of independent experiments	Affinity constant (M^{-1}) $\times$ 10^{-6}	Number of sites (relative units)
AGRGDSPK(VLA-5 ligand)	None	4	1.86 ± 0.67	0.28 ± 0.12
AGRGDSPK	K20	2	1.81 ± 0.16	0.15 ± 0.06
AEILDVPST(VLA-4 ligand)	None	4	6.94 ± 9.43	0.15 ± 0.04
AEILDVPST	K20	2	5.22 ± 1.22	0.08 ± 0.04

Monocytic THP-1 cells were incubated with synthetic fluorescent integrin ligands and assayed with flow cytometry for determination of the affinity constant and site number as described in Materials and Methods. Mean values of separate experiments are shown ± SE of the mean.

ment might involve two complexes with respective dissociation rates of 5.1 s^{-1} and 0.137 s^{-1}, and respective proportions of 66% and 34%. In any case, the most frequent event after integrin/fibronectin encounter seems to be the formation of a transient complex with a dissociation rate close to 4–5 s^{-1}. This is in contrast with recent studies made on complexes formed between truncated $\alpha5\beta1$ and wild-type or mutated fibronectin: the dissociation rate was 0.0065 s^{-1} and 0.0113 s^{-1}, respectively, when fibronectin bore or was deprived of an active synergy site (Takagi et al., 2003). Also, the force-free separation of fibronectin and $\alpha5\beta1$ integrin was, respectively, estimated at 0.13 s^{-1} and 0.012 s^{-1} with high- or low-affinity state integrin (Li et al., 2003). The simplest interpretation of this apparent discrepancy would be that the transient binding events we reported could not be detected with other methods based on surface plasmon resonance (Takagi et al., 2003) or atomic force microscopy (Li et al., 2003). Indeed, the contact time between interacting molecules is of the order of 1 ms under our experimental conditions (i.e., bond range of ≈10 nm divided by the relative membrane-to-surface velocity of ≈10 μm/s). In contrast, contact duration in the aforementioned experiments might range between several hundreds of seconds (Takagi et al., 2003) and 50 ms or more (Li et al., 2003). It may be emphasized that a similar disclosure of previously undetected short interactions was recently reported by Smith et al. (1999) when they studied selectin-ligand interaction under flow with a rapid video camera.

Because the ''bond-stabilization'' and the ''two-complex'' model can yield quite similar detachment curves after proper parameter fitting, it seems very difficult to find a formal way of discriminating between these models. However, we tend to favor the bond-stabilization model because treatments supposed to change integrin accessibility without altering their conformation did not modify the shape of detachment curves, whereas they might be expected to change the proportion of independent complexes. Indeed, exposure to neutral K20 antibody or microfilament inhibition, resulted in a decrease of binding efficiency without any alteration of detachment kinetics. The decrease of binding frequency after K20 treatment (Table 2) may be ascribed to a steric hindrance that should be particularly effective under flow conditions, due to the briefness of molecular encounter. It may seem surprising that cytochalasin D and latrunculin A decreased binding frequency. Because detachment curves were not altered by these drugs, the simplest interpretation might be that receptor accessibility be altered, possibly by a change of cell shape and/or receptor repartition between cell surface protrusions and other membrane regions, because such variations were suggested to alter integrin function (Erlandsen et al., 1993).

The effect of 12G10 antibody is more difficult to understand: indeed, in view of previous evidence, function-activating antiintegrin antibodies might be expected to increase the rate of bond formation (Cai and Wright, 1995; Li et al., 2003; Takagi et al., 2003), as well as decrease the rate of bond dissociation (Chigaev et al., 2001; Li et al., 2003). Therefore, it was surprising that this antibody did not promote multiple-bond formation at least on surfaces coated with high-fibronectin density. However, this conclusion was supported by two independent arguments, i.e., the lack of increase of bond frequency (Table 2, first and fourth data rows) and analysis of detachment curves. This might be due to a steric effect precluding multiple-bond formation. Indeed, due to the short duration of molecular encounter, steric hindrance may be more apparent under flow than under conditions used by other authors, in accordance with the inhibitory effect of supposedly neutral K20 antibody on bond formation (Table 2).

It seems, therefore, warranted to ascribe the slower release of cells bound to surfaces coated with higher fibronectin densities to the formation of multiple bonds. Because the slightly better fit obtained with the initial bond-formation model, as compared to continuous bond-formation model (Fig. 5) is not sufficient to rule out the latter model, it is useful to emphasize additional support for our preference to the initial bond-formation model; the delay required for bond formation when a fibronectin molecule is within binding distance of the cell membrane is certainly much less than one second. Indeed, because the size of a receptor is of the order of 10 nm, the local fibronectin concentration near the receptor would be of the order of $1/[N \times (10\ \text{nm})^3] = 0.0017$ M, where N is the Avogadro-Loschmidt number. Because the kinetic constant of the integrin-ligand association is of the order of 10^6 M^{-1} s^{-1} (Chen et al., 1999), bond formation would require <1 ms. Note that although the aforementioned estimates were obtained on soluble molecules, similar amounts of time are expected to be involved in

bond formation between free and surface-attached molecules provided free receptor rotation is allowed (Pierres et al., 1998). The only consequence of receptor attachment to a surface, as compared to soluble molecules, would be a possible reduction of the maximum number of bonds due to limitation of the number of available molecular orientations. Note that this initial bond-formation model was also found to hold in a recent study of the microkinetics of streptavidin-biotin association (Pierres et al., 2002).

Given that K20 antibody did not change the intrinsic fibronectin-integrin interaction, as showed by dynamic adhesion and flow cytometry measurements, it is reasonable to conclude that the increase of attachment duration caused by receptor clustering was due to an increase of the bond number.

That integrin-fibronectin association appeared as a multistep event is only one more consequence of the complexity of energy landscapes of ligand-receptor complexes that were disclosed by many reports on the interaction between antigen and antibodies (Pierres et al., 1995), avidin or streptavidin and biotin (Merkel et al., 1999; Pierres et al., 2002), L-selectin (Evans et al., 2001), or integrins (Zhang et al., 2002; Li et al., 2003). In this respect, it is interesting to compare our results to a thorough report on the rupture of $\alpha5\beta1$ integrin-fibronectin interaction with an atomic force microscope (Li et al., 2003) that appeared while this work was in progress. Integrin-expressing K562 cells were pushed by a force of the order of 100 pN against surfaces coated with fibronectin fragments. By examining the dependence of the rupture force on loading rate, the authors concluded that the detachment path displayed two barriers located at 0.41 and 0.086 nm from bound state (Merkel et al., 1999). The unstressed passage frequency of the external barrier was 0.13 s^{-1} in absence of activation. It would be tempting to speculate that our method revealed a weaker more external barrier, with a dissociation rate of 3.6 s^{-1}, in accordance with our previous suggestion (Pierres et al., 2002). However, more extensive studies are required to determine whether it is tenable to view ligand-receptor association/dissociation as a one-dimensional displacement along a major valley of the energy landscape, or the existence of multiple reaction paths might require a new theoretical framework to interpret experimental data.

Because our results revealed significant but limited quantitative effect of receptor clustering on cell adhesion microkinetics, it was important to get a rough estimate of the amount of clustering triggered by our treatment, to determine whether moderate binding changes were due to moderate or on the contrary extensive alteration of receptor distribution on the cell membrane. Although electron microscopy combined with gold labeling indeed allowed Detmers et al. (1987) to demonstrate a microclustering of integrin receptors, this approach is not well suited to the quantification of this phenomenon, due to the length of data acquisition, and possible artifacts related to cell fixation procedure. Indeed, confocal microscopy has long been used to monitor receptor aggregation (van Kooyk et al., 1994; Stewart et al., 1998) but we felt it useful to assess the significance of images because some caveats are useful to avoid misinterpretation; indeed, as demonstrated in our study, the bright points that are viewed on fluorescence images may represent only a minor fraction of cell surface fluorescent molecules, and only the image histogram can yield reliable information on the distribution of fluorescence molecules. However, there remains a problem when a given picture element (or pixel) representing an elementary volume element (i.e., a voxel) contains several molecules; hence, it is not possible to discriminate between 10 isolated molecules or five doublets located in the same voxel, except by using variance analysis. This is the reason why the median fluorescence index we reported could not be used as a fully quantitative estimate of receptor aggregation.

Our study of receptor affinity with fluorescent ligands deserves some comments: although several authors succeeded in estimating receptor affinity with flow cytometry (Chigaev et al., 2001), many difficulties must be overcome to tackle low-affinity specific binding and high nonspecific interaction. The linear approximation we used seemed to provide a convenient alternative to conventional blockade of specific binding with high amounts of unlabeled peptide (not shown). In any case, our conclusion that THP-1 cells displayed low-affinity fibronectin receptors is in line with a previously reported conclusion (Faull et al., 1993) that hemopoietic cells usually display low-activity β-1 integrins. Although it might be interesting to perform further experiments to study the increase of integrin affinity in stimulated cells, it must be emphasized that: i), in preliminary experiments, we found it difficult to increase β-1 integrin affinity in THP-1 cells (not shown), ii), our conditions were probably relevant, because we were mainly interested in the initial binding events involving unstimulated cells, and iii), although our results emphasized the importance of receptor accessibility and short-lived binding complexes, the flow cytometry approach is expected to yield information on the affinity of stabilized states. Results obtained with flow cytometry and the flow chamber are therefore not expected to be comparable. Thus, it was not warranted to plan an exhaustive comparison of the results obtained with both methods before all methodological problems were settled.

A question raised by our experiments was to know whether the adhesiveness differences of surfaces treated with different amounts of fibronectin were fully explained by fibronectin surface densities. When fibronectin-coated surfaces were examined with atomic force microscopy (not shown), surfaces coated with 1 μg/ml and 0.1 μg/ml fibronectin appeared quite similar, whereas surfaces exposed to 10 μg/ml fibronectin exhibited substantially higher roughness. Thus, the topography of surface-attached adhesion molecules might influence adhesive behavior as well as surface density.

The main conclusion of our work is that efficient attachment of THP-1 cells to extracellular matrix proteins might require simultaneous formation of several incomplete bonds rather than a single complete molecular interaction. The reason for this finding would be that, although a single complete bond may be strong and durable enough to immobilize a cell for a sufficient period of time to allow additional bond formation, the formation of a stable bond requires a fairly prolonged contact that is not always provided by mobile cells. This may explain the importance of receptor clustering for receptor efficiency, and account for possible discrepancies between receptor avidity and affinity.

We thank the Association pour la recherche sur le cancer and Conseil Régional Provence Alpes Côte d'Azur for a grant allowing the purchase of an atomic force microscope.

REFERENCES

Alon, R., D. A. Hammer, and T. A. Springer. 1995. Lifetime of P-selectin-carbohydrate bond and its response to tensile force in hydrodynamic flow. *Nature.* 374:539–542.

André, P., A. M. Benoliel, C. Capo, C. Foa, M. Buferne, C. Boyer, A. M. Schmitt-Verhulst, and P. Bongrand. 1990. Use of conjugates made between a cytolytic T cell clone and target cells to study the redistribution of membrane molecules in contact areas. *J. Cell Sci.* 97:335–347.

Cai, T. Q., and S. D. Wright. 1995. Energetics of leukocyte integrin activation. *J. Biol. Chem.* 270:14358–14365.

Chen, A., and V. T. Moy. 2000. Cross-linking of cell surface receptors enhances cooperativity of molecular adhesion. *Biophys. J.* 78:2814–2820.

Chen, L. L., A. Whitty, R. R. Lobb, S. P. Adams, and R. B. Pepinsky. 1999. Multiple activation states of integrin alpha 4 - beta 1 detected through their different affinities for a small molecule ligand. *J. Biol. Chem.* 274:13167–13175.

Chigaev, A., A. M. Blenc, J. V. Braaten, N. Kumaraswamy, C. L. Kepley, J. R. P. Andrews, J. M. Oliver, B. S. Edwards, E. R. Prossnitz, R. S. Larson, and L. A. Sklar. 2001. Real time analysis of the affinity regulation of alpha 4-integrin. *J. Biol. Chem.* 276:48670–48678.

Condic, M. L., and P. C. Letourneau. 1997. Ligand-induced changes in integrin expression regulates neuronal adhesion and neurite outgrowth. *Nature.* 389:852–856.

Cozens-Roberts, C., D. A. Lauffenburger, and J. A. Quinn. 1990. Receptor-mediated cell attachment and detachment kinetics. I. Probabilistic model and analysis. *Biophys. J.* 58:841–856.

Danilov, Y. N., and R. L. Juliano. 1989. Phorbol ester modulation of integrin-mediated cell adhesion: a postreceptor event. *J. Cell Biol.* 108:1925–1933.

Detmers, P. A., S. D. Wright, E. Olsen, B. Kimball, and Z. A. Cohn. 1987. Aggregation of complement receptors of human neutrophils in the absence of ligand. *J. Cell Biol.* 105:1137–1145.

Dwir, O., G. S. Kansas, and R. Alon. 2001. Cytoplasmic anchorage of L-selectin controls leukocyte capture and rolling by increasing the mechanical stability of the selectin tether. *J. Cell Biol.* 155:145–156.

Erlandsen, S. L., S. R. Hasslen, and R. D. Nelson. 1993. Detection and spatial distribution of the α2-integrin (Mac-1) and L-selectin (LECAM-1) adherence receptors on human neutrophils by high-resolution field emission SEM. *J. Histochem. Cytochem.* 41:327–333.

Evans, E., A. Leung, D. Hammer, and S. Simon. 2001. Chemically distinct transition states govern rapid dissociation of single L-selectin bonds under force. *Proc. Natl. Acad. Sci. USA.* 98:3784–3789.

Faull, R. J., N. L. Kovach, J. M. Harlan, and M. H. Ginsberg. 1993. Affinity modulation of integrin alpha5 beta1: regulation of the functional response by soluble fibronectin. *J. Cell Biol.* 121:155–162.

Gailit, J., J. H. Xu, H. Bueller, and R. A. F. Clark. 1996. Platelet-derived growth factor and inflammatory cytokines have differential effects on the expression of integrins alpha 1 beta 1 and alpha 5 beta 1 by human dermal fibroblasts in vitro. *J. Cell. Physiol.* 169:281–289.

Grabovsky, V., S. Feigelson, C. Chen, D. A. Bleijs, A. Peled, G. Cinamon, F. Baleux, F. Arenzana-Seisdedos, T. Lapidot, Y. van Kooyk, R. L. Lobb, and R. Alon. 2000. Subsecond induction of alpha 4 integrin clustering by immobilized chemokines stimulates leukocyte tethering and rolling on endothelial vascular cell adhesion molecule 1 under flow conditions. *J. Exp. Med.* 192:495–505.

Hato, T., N. Pampori, and S. J. Shattil. 1998. Complementary roles for receptor clustering and conformational change in the adhesive and signaling functions of integrin alpha IIb beta 3. *J. Cell Biol.* 141:1685–1695.

Hermanowski-Vosatka, A., P. A. Detmers, O. Götze, S. C. Silverstein, and S. D. Wright. 1988. Clustering of ligand on the surface of a particle enhances adhesion to receptor-bearing cells. *J. Biol. Chem.* 263:17822–17827.

Jagels, M. A., J. D. Chambers, K. E. Arfors, and T. E. Hugli. 1995. C5a- and tumor necrosis factor-alpha-induced leukocytosis occurs independently of beta 2 integrins and L-selectin: differential effects on neutrophil adhesion molecule expression in vivo. *Blood* 85:2900–2909.

Kaplanski, G., C. Farnarier, O. Tissot, A. Pierres, A-M. Benoliel, M-C. Alessi, S. Kaplanski, and P. Bongrand. 1993. Granulocyte-endothelium initial adhesion. Analysis of transient binding events mediated by E-selectin in a laminar shear flow. *Biophys. J.* 64:1922–1933.

Kasirer-Friede, A., J. Ware, L. Leng, P. Marchese, Z. M. Ruggieri, and S. J. Shattil. 2002. Lateral clustering of platelet GP-IB-IX complexes leads to up-regulation of the adhesive function of integrin alphaIIbbeta 3. *J. Biol. Chem.* 277:11949–11956.

Kucik, D. F., M. L. Dustin, J. M. Miller, and E. J. Brown. 1996. Adhesion-activating phorbol ester increases the mobility of leukocyte integrin LFA-1 in cultured lymphocytes. *J. Clin. Invest.* 97:2139–2144.

Lawrence, M. B., and T. A. Springer. 1991. Leukocytes roll on a selectin at physiologic flow rates: distinction from and prerequisite for adhesion through integrins. *Cell.* 65:859–873.

Leid, J. G., D. A. Steeber, T. F. Tedder, and M. A. Jutila. 2001. Antibody binding to a conformation-dependent epitope induces L-selectin association with the detergent resistant cytoskeleton *J. Immunol.* 166: 4899–4907.

Li, F., S. D. Redick, H. P. Erickson, and V. T. Moy. 2003. Force measurements of the alpha5beta1 integrin-fibronectin interaction. *Biophys. J.* 84:1252–1262.

Li, X., D. A. Steeber, M. L. K. Tang, M. A. Farrar, R. M. Perlmutter, and T. F. Tedder. 1998. Regulation of L-selectin-mediated rolling through receptor dimerization. *J. Exp. Med.* 188:1385–1390.

Lino, R., I. Koyama, and A. Kusumi. 2001. Single molecule imaging of green fluorescent proteins in living cells: E-cadherin forms oligomers on the free cell surface. *Biophys. J.* 80:2667–2677.

Ma, Q., M. Shimaoka, C. Lu, H. Jing, C. V. Carman, and T. A. Springer. 2002. Activation-induced conformational changes in the I domain region of lymphocyte function associated antigen 1. *J. Biol. Chem.* 277:10638–10641.

Maheshwari, G., G. Brown, D. Lauffenburger, A. Wells, and L. G. Griffith. 2000. Cell adhesion and motility depend on nanoscale RGD clustering. *J. Cell Sci.* 113:1677–1686.

Masson-Gadais, B., A. Pierres, A. M. Benoliel, P. Bongrand, and J. C. Lissitzky. 1999. Integrin alpha and beta subunit contribution to the kinetic properties of alpha 2-beta 1 collagen receptors on human keratinocytes analyzed under hydrodynamic conditions. *J. Cell Sci.* 112:2335–2345.

Merkel, R., P. Nassoy, A. Leung, K. Ritchie, and E. Evans. 1999. Energy landscapes of receptor-ligand bonds explored with dynamic force spectroscopy. *Nature* 397:50–53.

Miller, J., R. Knorr, M. Ferrone, R. Houdei, C. P. Carron, and M. L. Dustin. 1995. Intercellular adhesion molecule-1 dimerization and its consequences for adhesion mediated by lymphocyte function associated-1. *J. Exp. Med.* 182:1231–1241.

Mishell, B. B., and S. M. Shiigi. 1980. Selected Methods in Cellular Immunology. W. H. Freeman & Co., San Francisco, CA.

Mould, A. P., and M. J. Humphries. 1991. Identification of a novel recognition sequence for the integrin alpha 4 beta 1 in the COOH-terminal heparin-binding domain of fibronectin. *EMBO J.* 10:4089–4095.

Nie, S. M., D. T. Chiu, and R. N. Zare. 1994. Probing individual molecules with confocal fluorescence microscopy. *Science.* 266:1018–1021.

Pierres, A., A. M. Benoliel, and P. Bongrand. 1995. Measuring the lifetime of bonds made between surface-linked molecules. *J. Biol. Chem.* 270:26586–26592.

Pierres, A., A. M. Benoliel, and P. Bongrand. 1996. Measuring bonds between surface-associated molecules. *J. Immunol. Methods.* 196:105–120.

Pierres, A., A. M. Benoliel, and P. Bongrand. 1998. Studying receptor-mediated cell adhesion at the single molecule level. *Cell Adhes. Commun.* 5:375–395.

Pierres, A., A. M. Benoliel, C. Zhu, and P. Bongrand. 2001. Diffusion of microspheres in shear flow near a wall: use to measure binding rates between attached molecules. *Biophys. J.* 81:25–42.

Pierres, A., O. Tissot, B. Malissen, and P. Bongrand. 1994. Dynamic adhesion of CD8-positive cells to antibody-coated surfaces the initial step is independent of microfilaments and intracellular domains of cell-binding molecules. *J. Cell Biol.* 125:945–953.

Pierres, A., D. Touchard, A. M. Benoliel, and P. Bongrand. 2002. Dissecting streptavidin-biotin interaction with a laminar flow chamber. *Biophys. J.* 82:3214–3223.

Sabri, S., M. Soler, C. Foa, A. Pierres, A. M. Benoliel, and P. Bongrand. 2000. Glycocalyx modulation is a physiological means of regulating cell adhesion. *J. Cell Sci.* 113:1589–1600.

Sako, D., X-J. Chang, K. M. Barone, G. Vachino, H. M. White, G. Shaw, G. M. Veldman, K. M. Bean, T. J. Ahern, B. Furie, D. A. Cumming, and G. R. Larsen. 1993. Expression cloning of a functional glycoprotein ligand for P-selectin. *Cell* 75:1179–1186.

Scatchard, G. 1949. The attractions of proteins for small molecules and ions. *Ann. N. Y. Acad. Sci.* 51:660–672.

Seifert, U. 2000. Rupture of multiple parallel molecular bonds under dynamic loading. *Phys. Rev. Lett.* 84:2750–2753.

Shapiro, L., A. M. Fannon, P. D. Kwong, A. Thompson, M. S. Lehman, G. Grübel, J. F. Legrand, J. Als-Nielsen, D. R. Colman, and W. A. Hendrickson. 1995. Structural basis of cell-cell adhesion by cadherins. *Nature.* 374:327–337.

Skelton, T. P., C. Zeng, A. Nocks, and I. Stamenkovic. 1998. Glycosylation provides both stimulatory and inhibitory effects on cell surface and soluble CD44 binding to hyaluronan. *J. Cell Biol.* 14:431–446.

Smith, M. J., E. L. Berg, and M. B. Lawrence. 1999. A direct comparison of selectin-mediated transient, adhesive events using high temporal resolution. *Biophys. J.* 77:3371–3383.

Snedecor, G. W., and W. G. Cochran. 1980. Statistical Methods, 7th Ed. Iowa State Univ. Press. Ames, IA.

Stewart, M. P., A. McDowall, and N. Hogg. 1998. LFA-1-mediated adhesion is regulated by cytoskeletal restraint and by a Ca2+-dependent protease, calpain. *J. Cell Biol.* 140:699–707.

Stripack, D. G., E. Li, S. A. Silleti, J. A. Kehler, R. L. Geahlen, K. Hahn, G. R. Nemerow, and D. A. Cheresh. 1999. Matrix valency regulates integrin-mediated lymphoid adhesion via Syk kinase. *J. Cell Biol.* 144:777–787.

Takagi, J., K. Strokovich, T. A. Springer, and T. Walz. 2003. Structure of integrin alpha 5 beta 1, in complex with fibronectin. *EMBO J.* 22:4607–4615.

Takaki, Y., N. Seki, S. I. Kawabata, S. Iwanaga, and T. Muta. 2002. Duplicated binding sites for (1->3) -beta-D-glucan in the horseshoe crab coagulation factor G: implications for a molecular basis of the pattern recognition in innate immunity. *J. Biol. Chem.* 277:14281–14287.

Tissot, O., A. Pierres, C. Foa, M. Delaage, and P. Bongrand. 1992. Motion of cells sedimenting on a solid surface in a laminar shear flow. *Biophys. J.* 61:204–215.

Tsuchiya, S., M. Yamabe, Y. Yamaguchi, Y. Kobayashi, T. Konno, and K. Tada. 1980. Establishment and characterization of a human acute monocytic leukemia cell line (THP-1). *Int. J. Cancer.* 26:171–176.

Van de Winkel, J. G., R. van Omnen, T. W. J. Huizinga, M. A. H. V. M. de Raad, W. B. Tuijman, P. J. T. A. Groenen, P. J. A. Capel, R. A. P. Koene, and W. J. M. Tax. 1989. Proteolysis induces increased binding affinity of the monocyte type II FcR for human IgG. *J. Immunol.* 143:571–578.

Van Kooyk, Y., and C. G. Figdor. 2000. Avidity regulation of integrins: the driving force in leukocyte adhesion. *Curr. Opin. Cell Biol.* 12:542–547.

Van Kooyk, Y., P. Weder, K. Heije, and C. J. Figdor. 1994. Extracellular Ca2+ modulates leukocyte function-associated antigen-1 cell surface distribution on T lymphocytes and consequently affects cell adhesion. *J. Cell Biol.* 124:1061–1070

Wayner, E. A., A. Garcia-Pardo, M. J. Humphries, J. A. McDonald, and W. J. Carter. 1989. Identification and characterization of the T lymphocyte adhesion receptor for an alternative cell attachment domain (CS-1) in plasma fibronectin. *J. Cell Biol.* 109:1321–1330.

Yap, A. S., W. M. Brieher, M. Pruschy, and B. M. Gumbiner. 1997. Lateral clustering of the adhesive ectodomain: a fundamental determinant of cadherin function. *Curr. Biol.* 7:308–315.

Zhang, X., E. Vojcikiewicz, and V. T. Moy. 2002. Force spectroscopy of the leukocyte function associated antigen-1/intercellular adhesion molecule 1 interaction. *Biophys. J.* 83:2270–2279.

Zhu, C., M. Long, S. E. Chesla, and P. Bongrand. 2002. Measuring receptor/ligand interaction at the single bond level: experimental and interpretative issues. *Ann. Biomed. Engineering* 30:305–314.